Stability of Turning Processes with Actively Controlled Linear Motor Feed Drives

D. M. Alter
Graduate Student.

Tsu-Chin Tsao
Assistant Professor.

Department of Mechanical and Industrial Engineering,
University of Illinois at Urbana-Champaign,
Urbana, IL 61801

Using linear motors as machine tool feed drives has the potential of enhancing machining performance by eliminating gear related mechanical problems and increasing speed and accuracy, but introduces a stability concern due to a strong dynamic feedback interaction between the machining process and the drives. This paper investigates the stability aspect of this dynamic interaction and the use of active damping to achieve machining stability in turning. Various necessary and sufficient conditions for stability at all cutting speeds are derived, and have been used to study the effect of damping and gear reduction in system stability. The interaction of the cutting process with the tool servo loop is seen to have significant instability consequences in systems with small drive gear reductions. Both theoretical stability and experimental cutting results are presented for PD and PID regulation. Results show that actively controlled linear motors can provide sufficient dynamic stiffness for stable turning operation.

1 Introduction

One crucial component for high-speed machining applications is the development of machine tool feed drives and motion controls that are capable of high-speed precision motion. At present, most metal cutting machine tools consist of lead-screw/ballnut-type gear trains to convert, for each axis, the prime mover rotary motion into the cutting tool or workpiece linear motion. Such mechanical transmissions not only significantly reduce the linear motion speed and the dynamic response, but also introduce backlash, large frictional and inertial loads, and structural flexibility. However, these gear reductions do offer the advantage of isolating the prime mover from the cutting process so that cutting forces may be ignored under normal cutting conditions.

To increase the feedrate and the response for high-speed precision machining, it is necessary to reduce the gear ratio, and to ultimately use direct-drives. Direct-drive actuators can have faster speed and dynamic responses, and eliminate gear related problems as well. Furthermore, unique features such as dynamic error compensation and active chatter/vibration suppression can be readily employed by the servo control software without the need for altering hardware. Therefore, direct drives have good potentials for next generation high-speed machine tool feed axes. However, the use of direct-drives introduces a stability concern due to the dynamic interaction between the cutting process and the servo drive.

Stability is a fundamental issue in studying any dynamical system. When investigating the possibility of using direct-drive linear motors for machine tool feed motion, the overall machining system stability is the first issue to be addressed before any of the aforementioned potentials can be investigated. This paper is mainly concerned with the machining stability problem introduced by the dynamic interactions between the machining process and the servo controlled direct-drives.

Some previous use of direct drive actuators for turning has been made in the past 25 years. In the late 1960's, some work on active control of the direct-drive turning process was performed (Comstock et al., 1969; Nachtigal and Cook, 1970; Nachtigal, 1972). These efforts utilized either position feedback or force feedback to perform circular cutting with an electro-hydraulic tool actuator. The results showed the significant stability improvements possible with active cutting control. Comstock's work, however, neglected the effect of the cutting forces on cutting tool motion, while Nachtigal's work essentially used a feedforward control design to match the drive dynamics to the lathe/workpiece structure dynamics. Mitchell and Harrison later investigated the disturbance rejection capabilities of the previous control schemes, and theoretically formulated an observer based state feedback controller (Mitchell and Harrison, 1974, 1977).

It is important to note that the dynamic characteristics of direct drive actuators vary depending upon which specific type is employed. The present use of a linear motor actuator is motivated by its substantial savings in weight, bulk, noise, maintenance, and cost potential over hydraulic systems (Barkman, 1980). Unlike a hydraulic actuator, a linear motor has zero static stiffness. Active control is therefore necessary for proper functioning.

The remainder of this paper is organized as follows. In Section 2, the dynamic interactions between each of the machining system elements are formulated and the role of gear ratio in system stability is discussed. In Section 3, closed loop servo control design issues for stable machining operations are discussed. In Section 4, a numerical simulation study is de-

Contributed by the Production Engineering Division for publication in the JOURNAL OF ENGINEERING FOR INDUSTRY. Manuscript received Jan. 1993; revised May 1993. Associate Technical Editor: S. Kapoor.

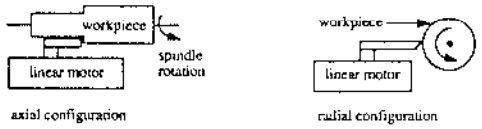

Fig. 2.1 Cutting configurations

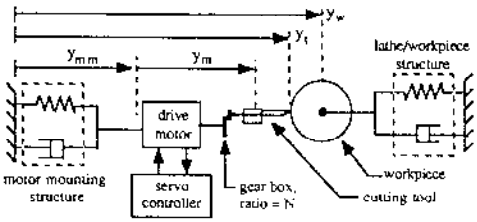

Fig. 2.2 Generalized cutting system schematic

scribed. In Section 5, a direct-drive motor experimental system is described and experimental turning results for both stable and unstable cutting are demonstrated. Finally, conclusions are given in Section 6.

2 System Dynamic Model

The goal of any machining process is the removal of metal from the workpiece such that some desired workpiece geometry is achieved with good surface finish. Chatter instability caused by cutting process feedback leaves ripple marks and indentations on the workpiece surface, and may cause tool or workpiece breakage. The conventional approach to combat chatter has been the construction of lathes with very high static stiffness along the cutting axes, as will be discussed in Section 3.1. In a lathe system, flexibility exists in geared drives, lathe bearings, and mounting structures. Additionally, certain workpiece geometries, such as the turning of a long slender rod, further decrease system static stiffness. While the directly driven lathe system does not suffer from gear flexibility and backlash, the direct drive (e.g., linear motor) itself becomes the most flexible element in the system along its primary axis of motion. Two possible circular cutting configurations are shown in Fig. 2.1. Theoretical formulations will assume the radial configuration, although the axial formulation is essentially identical.

The machining system, which consists of the machining process, feed drives and servo controllers, and workpiece and machine structures, may be modeled as suggested by Fig. 2.2. The motor mounting structure and lathe/workpiece structure account for flexibility in the machine base structures, as well as in the workpiece itself. It should be noted that these structures are not necessarily simple spring-damper systems; rather they are likely to be distributed systems. By neglecting the motor mounting structure for convenience of presentation, the closed loop system block diagram is shown in Fig. 2.3. The notation $(\cdot)$ represents a general nonlinear time-varying input-output operator. The cutting process dynamics from depth of

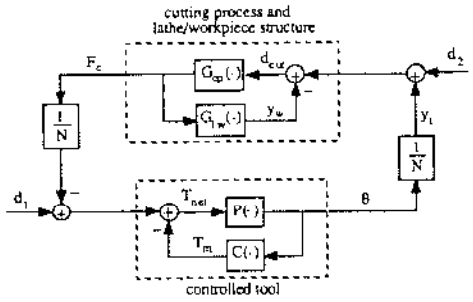

Fig. 2.3 General feedback loop block diagram

cut to cutting force are denoted by $G_{cp}(\cdot)$, the lathe/workpiece dynamics from force input to position output are denoted by $G_{lw}(\cdot)$, and the drive motor dynamics from torque input to position output are denoted by $P(\cdot)$. The servo controller (includes the servo-amplifier) $C(\cdot)$ produces a torque input to the motor using motor position as its input (as opposed to tool position). External input signal d_1 represents a torque disturbance acting on the drive motor, while external input d_2 represents a positional disturbance in the cutting depth, for example from spindle runout or workpiece out of roundness. Note that in the case of a linear motion drive, the torques T_m, T_{net}, and d_1, and angular position θ should instead be considered as forces and position, respectively, although such distinction is extraneous to current analysis. The units of "N" (i.e., the gearbox reduction, either from rotary to linear, or from linear to linear motion) are unspecified and thus one has the freedom to interchange force and torque.

If the drive motor and cutting tool are linear systems, any significant inertia and damping present in the cutting tool dynamics (i.e., those drive dynamics occurring after the gear box) may be incorporated into the drive dynamics $P(\cdot)$. The typically large stiffness of the cutting tool has been neglected. For example, assuming mass-damper structures for the drive motor and cutting tool leads to the following Laplace transfer function for $P(\cdot)$:

$$P(\cdot) = P(s) = \frac{\theta(s)}{T_{net}(s)} = \frac{1}{\left(J_m + \frac{m_t}{N^2}\right)s^2 + \left(B_m + \frac{B_t}{N^2}\right)s} \tag{2.1}$$

where J_m, and B_m denote motor inertia and damping, and m_t and B_t similarly denote tool properties.

Three feedback loops exist in the system: the feed drive servo loop, the tool-workpiece loop, and the outer loop that connects the first two loops. The tool-workpiece loop is the traditional machining stability loop considered in the literature (Smith and Tlusty, 1990; Srinivasan, 1982; Srinivasan and Nachtigal, 1977; Merritt, 1965; Gurney and Tobias; 1961). For conventional machine tools where gear reduction ratio N is large, the stability of this loop usually implies the stability of the entire system. Provided the servo loop is also designed stable, the

Nomenclature

B_l = lathe/workpiece damping
B_m = motor damping
B_t = tool damping
$C(\cdot)$ = servo controller operator
d_{cut} = depth of cut
d_w = workpiece diameter
F_a = motor actuation force
F_c = cutting force
$G_{cp}(\cdot)$ = cutting process operator
$G_{lw}(\cdot)$ = lathe/workpiece structure operator
J_m = motor inertia
K_c = static cutting stiffness
K_{cd} = dynamic cutting stiffness
K_l = lathe/workpiece stiffness
m_l = lathe/workpiece mass
m_t = tool mass
N = drive motor gear reduction
$P(\cdot)$ = effective drive system operator
s = Laplace Transform variable
T_m = drive motor torque
T_{net} = net input torque to drive system
y_t = tool position
y_w = workpiece position
μ = cutting overlap factor
θ = drive motor angular position
τ = time per workpiece revolution

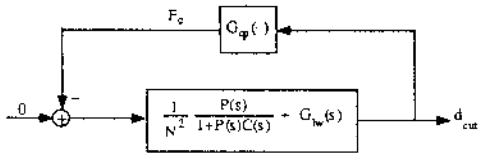

Fig. 3.1 Equivalent block diagram to Fig. 2.3

stability of the outer loop can easily be achieved because its loop gain, being divided by N^2, is small. In other words, for sufficiently large N, the servo loop is effectively decoupled from the tool-workpiece loop by the small gains of the two $1/N$ blocks. For high-speed machines where N is small, or with direct drives where $N = 1$, this drive-process interaction loop must be accounted for in the system stability analysis. This paper will focus on the stability of this process-drive feedback loop which has not been of much consideration before.

3 Closed Loop Stability Analysis

It is reasonable to assume linear structures for the servo loop and lathe/workpiece dynamics since such hardware is typically linear (albeit of possibly high order). By isolating the cutting process from the rest of the system, Fig. 2.3 can be redrawn to give Fig. 3.1, where the notation (s) represents Laplace transform. Both blocks are intuitively assumed stable, but the cutting process may be nonlinear and time-varying. For an arbitrary signal $z(t)$, its L_2 signal norm is defined as

$$\|z\|_2 := \left(\int_{-\infty}^{+\infty} z(t)^2 \, dt \right)^{1/2} \tag{3.1}$$

Now consider the cutting process (or any other process) as all possible stable perturbations whose L_2 induced system gain is bounded by ρ, i.e.

$$\sup_{w} \frac{\|G_{cp}(\cdot)w\|_2}{\|w\|_2} < \rho \tag{3.2}$$

where $w(t)$ is an arbitrary input signal with $0 < \|w\|_2 < +\infty$. Note that for a linear time invariant system, the L_2 induced system gain is simply the H_∞ norm of the system transfer function. Define the transfer function of the servo loop from force input to position output as $T(s)$:

$$T(s) := \frac{P(s)}{1 + P(s)C(s)} \tag{3.3}$$

To conclude system stability, the small-gain theorem (Desoer and Vidyasagar, 1975) states that the system is L_2 stable if and only if

$$\left\| \frac{1}{N^2} T(j\omega) + G_{lw}(j\omega) \right\|_{H_\infty} = \max_{\omega \in \Re e} \left| \frac{1}{N^2} T(j\omega) + G_{lw}(j\omega) \right| < \frac{1}{\rho} \tag{3.4}$$

For sufficiently large N, condition (3.4) may be approximated as

$$\max_{\omega \in \Re e} |G_{lw}(j\omega)| < \frac{1}{\rho} \tag{3.5}$$

which is precisely a necessary and sufficient condition for stability of the tool-workpiece loop in Fig. 2.3. As mentioned before, this case has been afforded considerable attention in the literature. Condition (3.5) proves the stability argument given in the previous section, namely that in systems with large gear reductions, stability of the tool-workpiece loop typically implies stability of the entire system. Condition (3.5) also confirms the conventional wisdom that lathes with large stiffness (i.e. $|G_{lw}(j\omega)|$ small) are desirable for system stability. Finally, in light of (3.4), it is clear for large N that if the tool-workpiece loop is unstable, the servo controller present in $T(s)$ will not be able to stabilize the system due to the attenuating factor $1/N^2$.

Consider now the small N (e.g. direct drive) case. Equation (3.4) may be used to design a stabilizing servo controller for the machining system even if the tool-workpiece loop is unstable. As a simplification, consider the case where the tool-workpiece loop is of sufficient stiffness so that $|G_{lw}(j\omega)|$ may be neglected (this assumption will be made for the remainder of this section).

Defining the dynamic servo stiffness by

$$K_s := \min_{\omega \in \Re e} \frac{1}{|T(j\omega)|} \tag{3.6}$$

Equation (3.4) may now be approximated as

$$N^2 K_s > \rho \tag{3.7}$$

which means that the servo stiffness of the (direct) drive should be large enough to ensure stability. One possible control goal is therefore to minimize the H_∞ norm of $T(s)$. It also intuitively follows that enough damping should be present in the servo loop to avoid any large resonant peaks, which would reduce K_s. Satisfaction of condition (3.7) may be a significant challenge for $N = 1$.

Conditions (3.4) and (3.7) imposed on the direct drive system are rather general but also tend to be conservative since the cutting process is modeled as an operator of bounded gain, but otherwise arbitrary. Such conditions should be incorporated in the servo controller design for general purpose machine tools, where a variety of cutting processes and cutting conditions may be involved and thus are best characterized as an unstructured perturbation to the machine. For such a case, it is concluded that the dynamic servo stiffness K_s should be designed large. It might also be noted that large dynamic servo stiffness is of importance for good disturbance rejection performance, although this issue is not covered in this paper.

In special purpose machine tool design, the cutting process and conditions can be characterized more precisely, leading to refined stability conditions. For turning, the cutting model may be given by the transfer function

$$G_{cp}(s) = \frac{F_c}{d_{cut}} = K_c(1 - \mu e^{-\tau s}) - K_{cd}s \tag{3.8}$$

which characterizes the key primary and regenerative feedback mechanisms in the process (Matsubara et al., 1985). The many geometries and parameters involved in the cutting process, such as material composition, tool rake, lead, and back angle, width of cut, and tool nose radius, have all been lumped into the cutting constants K_c and K_{cd}. The cutting process damping $(K_{cd}s)$ may be absorbed into the machine tool dynamics such that the cutting process model becomes the often used "Classical" one, given by

$$G_{cp}(s) = K_c(1 - \mu e^{-\tau s}) \tag{3.9}$$

In real metal turning, the following constraints are placed on the parameters in (3.9):

(1) cutting load: $0 \le K_c \le K_{c,max}$
—dependent on workpiece material, tool condition, depth of cut and feedrate
(2) spindle speed range: $0 \le \tau_{min} \le \tau \le \tau_{max}$
(3) overlap factor: $0 \le \mu \le 1$

The case $K_c = 0$ represents noncutting servo motion, which must always be designed stable in any practical cutting system (i.e., $T(s)$ stable). Worst case cutting conditions from a stability point of view are represented by $\mu = 1$ and $K_c = K_{c,max}$, where $K_{c,max}$ must be determined a priori based upon expected cutting conditions. Under these constraints, it is not difficult to see

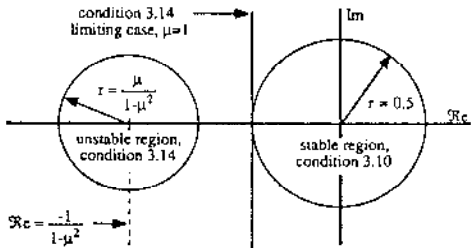

Fig. 3.2 Complex plane representation of conditions 3.10 and 3.14

from (3.9) that $\rho \le 2K_{c,max}$, and therefore a sufficient condition for system stability, according to (3.7), is that

$$N^2K_s > 2K_{c,max} \tag{3.10}$$

For the direct-drive system, this means that the servo stiffness should be at least twice the maximum expected static cutting stiffness.

Less conservative stability conditions may also be obtained. The characteristic equation that determines stability in Fig. 2.3 is

$$\Delta(s) = 1 + \frac{1}{N^2}\, T(s)G_{cp}(s) + G_{tw}(s)G_{cp}(s) = 0 \tag{3.11}$$

Recalling that the tool-workpiece loop is here neglected, and applying the cutting process model (3.9), the characteristic equation may be rearranged into the form

$$\Delta(s) = 1 - \mu e^{-\tau s}\, \frac{\frac{K_{c,max}}{N^2}\, T(s)}{1 + \frac{K_{c,max}}{N^2}\, T(s)} = 0 \tag{3.12}$$

If $1 + K_{c,max}T(s)/N^2$ is stable (i.e., the cutting system is closed loop stable in the absence of cutting process regeneration), the small gain theorem is again applicable so that the closed loop system (with cutting regeneration) is stable if and only if

$$\left| \frac{\frac{K_{c,max}}{N^2}\, T(j\omega)}{1 + \frac{K_{c,max}}{N^2}\, T(j\omega)} \right| \le \frac{1}{\mu} \tag{3.13}$$

Equation (3.13) is equivalent to (see Appendix A for derivation)

$$\left| \frac{K_{c,max}}{N^2}\, T(j\omega) + \frac{1}{1-\mu^2} \right| > \frac{\mu}{1-\mu^2} \tag{3.14}$$

Conditions (3.10) and (3.14) have graphical interpretations in the complex plane, as illustrated in Fig. 3.2. Condition (3.10) restricts $K_{c,max}T(j\omega)/N^2$ to an origin centered circle of radius 1/2. On the other hand, condition (3.14) requires the exclusion of $K_{c,max}T(j\omega)/N^2$ from a circular area in the complex plane, the center and radius depending on μ. For $\mu = 1$, this exclusion zone becomes the half plane to the right of $\Re e = -1/2$. At the other limiting case of $\mu = 0$, (3.14) may be interpreted as nonencirclement of the $-1+0j$ point on the Nyquist plot of $K_{c,max}T(j\omega)/N^2$. It is clear that (3.10) is much more conservative than (3.14).

The assumption that $1 + K_{c,max}T(s)/N^2$ be stable would seem to hamper the utility of condition (3.14) since there appears to be no guarantee that the assumption will hold upon completion of a design based on (3.14). However, since $T(s)$ must be stable and since $K_{c,max}N^2$ is stable, the Nyquist stability technique states that $1 + K_{c,max}T(s)/N^2$ is stable if and only if the Nyquist plot of $K_{c,max}T(j\omega)/N^2$ does not encircle the $-1+0j$ point. When performing design then, the simultaneous satisfaction on Fig. 3.2 of condition (3.14) along with nonencirclement of the $-1+0j$ point by $K_{c,max}T(j\omega)/N^2$ ensures the stability of the complete lathe system.

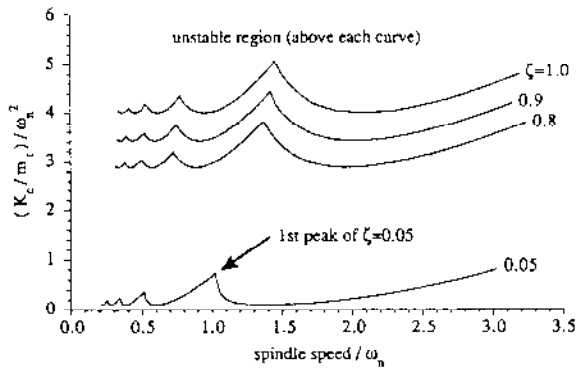

Fig. 3.3 Stability chart for use with PD controller, $\mu = 1$

A similar condition to (3.14) has previously been presented for stability of the tool-workpiece loop when neglecting the servo dynamics (Merritt, 1965). Finally, note that all of the stability conditions presented in this section determine stability without explicit use of spindle speed.

3.1 Stability Analysis for Linear Motor Lathe Drive-PID Control. Beyond the presented conditions in the previous section, further stability insight may be obtained by assuming model forms for every block in the system of Fig. 2.3. If structure flexibilities in the lathe/workpiece are neglected (i.e., $G_{tw}(s) = 0$), tool position may be treated as cutting depth. Additionally, the direct drive motor will be modeled as a linear mass-damper system, with $N = 1$, and with the cutting process damping incorporated into the motor damping. For the linear motor, the drive output torque T_m becomes a force, here denoted by F_a. The PID control law is given by:

$$F_a = K_p e(t) + K_d \dot{e}(t) + K_I \int_0^t e(\tau)\, d\tau \tag{3.15}$$

where the error signal is defined as $e(t) := y_{ref}(t) - y(t)$ with $y_{ref}(t)$ being the desired tool position. First consider the case with $K_I = 0$ (i.e., PD control). The closed loop transfer function is given as

$$\frac{d_{cut}}{d_{ref}} = \frac{K_d s + K_p}{m_t s^2 + (K_d + K_{cd} + B_t)s + K_p + K_c - \mu K_c e^{-\tau s}} \tag{3.16}$$

Equation (3.16) shows that PD control physically represents the mechanical addition of a spring and damper to the linear motor system. This is analogous to a passive lathe with 2nd order structure dynamics in either the cutting tool or workpiece, which has a characteristic equation of identical form.

The Nyquist stability technique has been applied by arranging the characteristic equation of (3.16) into the form:

$$1 + \frac{K_c}{m_t}\, \frac{1 - \mu e^{-\tau s}}{s^2 + 2\zeta\omega_n s + \omega_n^2} = 0 \tag{3.17}$$

where

$$K_P = m_t\omega_n^2, \quad K_d = 2m_t\omega_n\zeta - K_{cd} - B_t, \quad 0 \le \mu \le 1.$$

Figure 3.3 shows a nondimensional, characteristically lobed stability chart for several damping ratios and with $\mu = 1$, obtained from (3.17). Recall that the case $\mu = 1$ represents worst case stability. Each curve is lower bounded by a nondimensional cutting stiffness value below which operation is stable at all spindle speeds. This value is known as the asymptotic borderline of stability, and its behavior as a function of system parameters is given by Eq. (3.18) below (see Appendix B for derivation).

$$\frac{K_c}{m_t\omega_n^2}=\frac{2}{\mu^2}\left[\zeta^2+\sqrt{\mu^2+\zeta^2(1-\mu^2)}\;\zeta\right] \tag{3.18}$$

The asymptotic K_c monotonically increases with ζ, and monotonically decreases with μ, as can be verified. Note that the nondimensional cutting stiffness $K_c/m_t\omega_n^2$ is equivalent to K_c/K_p for the active control case and to K_c/K_t for the passive lathe. Equation (3.10) illustrated the importance of dynamic stiffness to stability, and in deriving (3.18), dynamic stiffness has been quantified in terms of static stiffness (i.e., K_p or K_t) and damping ratio by assuming 2nd order models for the servo loop (or the passive lathe).

A passive lathe typically exhibits $\zeta \approx 0.05$ (Merritt, 1965; Nachtigal, 1972) and a relatively high static stiffness for the structure dynamics (excluding the workpiece, which is not considered here in either the active control or passive case). Active control with the linear motor achieves greater damping, but lower static stiffness, both being limited by available motor force. Thus for a given μ, the asymptotic stability borderline will increase with the increase in damping, but then decrease with the reduction in stiffness. The proposed regulating controller achieves a net positive asymptotic stability gain over the passive lathe only if damping can be increased sufficiently to compensate for the decreased static stiffness.

It should be noted that while the above analysis utilizes damping and static stiffness, the root of the explanation stems from dynamic stiffness. Recall that dynamic stiffness has been defined as the inverse of the maximum magnitude of a systems frequency response. The frequency response plot for the lightly damped passive lathe will have a large resonant peak near its natural frequency, thus reducing its dynamic stiffness. The frequency response of the better damped active control case does not contain such a peak. Therefore, even though its frequency response plot may be higher than that of the passive lathe at most frequencies (i.e., other than near the passive lathes resonant peak), its dynamic stiffness can still be comparable with that of the passive lathe. According to (3.7), it is by this mechanism that direct drive cutting may be competitive with the passive lathe from a stability standpoint.

The only adjustable parameter in the passive system is the lathe spindle speed, and one approach has been to set this spindle speed near the first natural frequency of the lathe/workpiece structure (Merritt, 1965; Smith and Tlusty, 1990). This corresponds to operation in the region beneath the 1st peak of the $\zeta = 0.05$ stability curve in Fig. 3.3. Notice that for this curve, the ratio of the 1st peak nondimensional cutting stiffness to the asymptotic stability borderline is 7.0. Active PD control allows for the design of ζ and ω_n. The ratio of the 1st peak cutting stiffness multiplier to the asymptotic stability borderline for the $\zeta = 0.8, 0.9$, and 1.0 curves is approximately 1.3 in all three cases. Thus, for the second order system at these higher damping ratios, utilization of the larger stability region beneath the 1st peak gives little additional benefit over a conservative design using the asymptotic stability value, which also makes system stability essentially insensitive to spindle speed.

To increase the static stiffness for the active control case, integral control may be added as an extension of the PD control. With PID control, the characteristic equation of (3.17) becomes

$$1+\frac{K_c}{m_t}\frac{s(1-\mu e^{-\tau s})}{(s+a)(s^2+2\zeta\omega_n s+\omega_n^2)}=0 \tag{3.19}$$

where

$$K_p=m_t(2\zeta\omega_n a+\omega_n^2) \qquad K_I=m_t\omega_n^2 a$$
$$K_d=m_t(2\zeta\omega_n+a)-K_{cd}-B_t.$$

A Nyquist stability analysis reveals that the additional pole-zero combination of (3.19) quantitatively effects the PD asymptotic stability borderline as a scalar gain. The value of this gain depends on the selected damping ratio and on the ratio of the additional pole location to the natural frequency, as shown in Fig. 3.4. Note that with $a = 0$, (3.19) reduces to (3.17) and the gain of Fig. 3.4 becomes unity. The asymptotic stability borderline for PID control is seen greater than or equal to that of PD control. Theoretically speaking, the static stiffness by PID control should be infinite.

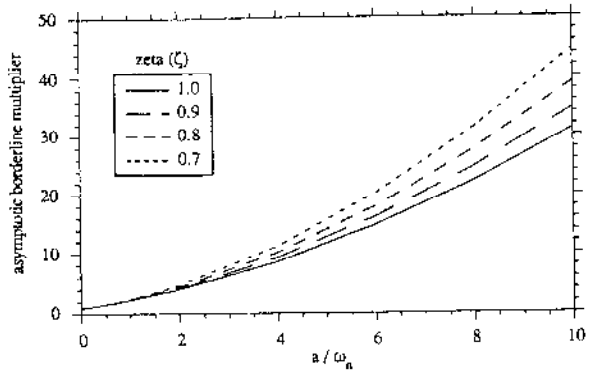

Fig. 3.4 Gain in PID asymptotic stability borderline over PD control, $\mu = 1$

4 Example Lathe System: Theoretical Stability and Simulation Result

A 2nd order lathe/workpiece structure representing the 1st vibratory mode was assumed and the following realistic system parameters used to analyze system performance (Thompson, 1986):

$$m_t = 164 \text{ kg} \quad B_t = 1810 \text{ N·s/m}$$
$$K_t = 2.0\text{E}6 \text{ N/m} \quad m_t = 9.5 \text{ kg} \quad \mu = 0.945$$

The PID controller was designed for the rigid lathe case given by Eq. (3.19): $\omega_n = 295$ rad/s, $\zeta = 0.544$, and $a = 93.3$ rad/s. Thus: $K_p = 1.1133\text{e}6$, $K_d = 3.9404\text{e}3$, $K_I = 7.7264\text{e}7$. Figure 4.1 shows theoretical stability limits for the following cases using the above given parameters:

case 1: passive lathe (fixed tool, 2nd order lathe flexibility)
case 2: PID control without the lathe dynamics
case 3: PID control with 2nd order lathe dynamics

As predicted from Figs. 3.3 and 3.4, case 2 shows a greater stability limit than case 1 for spindle speeds up to 3500 rpm. Beyond this spindle speed, higher vibratory modes for the lathe/workpiece should be considered before forming a conclusion. Case 3 shows that the introduction of lathe dynamics into the closed loop system reduces the stability margin from that of case 2 at all spindle speeds. However, this reduced stability margin is still greater than the passive lathe case. It is seen from the figure that at spindle speeds above 1600 rpm, the two active control cases give similar stability limits, implying that lathe dynamics may be neglected.

The natural frequency of the example passive lathe is 1054 rpm, and as stated in Section 3.1 and also apparent from Fig. 4.1, it is desirable to match the spindle speed of the passive system to this natural frequency in order to exploit the narrow band stability peak at this frequency. In comparison, the case 3 active control offers several wide, uniformly high stability limit bands between approximately 300 and 1054 rpm, and another usable stable region above 1600 rpm.

In an actual lathe system, both primary and regenerative cutting force is always positive (i.e., repelling the tool from the workpiece). With negative cutting depth, the cutting force becomes zero. The cutting process model (3.9) used in the determination of the theoretical stability limits of Fig. 4.1 does not account for this nonlinearity. To demonstrate this nonlin-

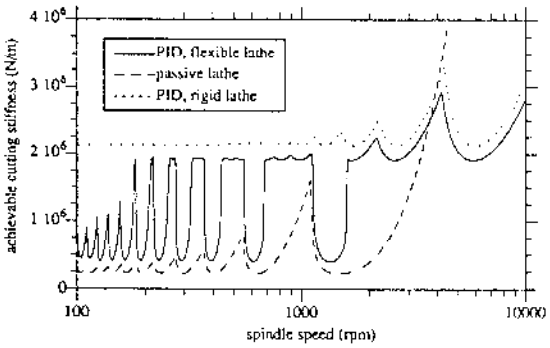

Fig. 4.1 Lobed stability plot, for example, lathe system

Table 4.2 Theoretical and simulated stability limits for the example lathe system at 800 rpm

$K_{c,max}$ (N/mm)

	passive lathe	PID, flexible lathe	PID, rigid lathe
theoretical	500	1900	2150
simulated	970	2800	3100

ear effect, simulation was performed with a discrete domain controller equivalent (see Eq. 5.1) with a sampling rate of 1000 Hz. The results showed the nonlinearity to have a stabilizing effect for both active and passive systems at all spindle speeds; shown in Table 4.2 for an 800 rpm spindle speed and 2 mm nominal cutting depth. Therefore, it should be safe to neglect this nonlinearity in the PID controller design.

5 Experimental Hardware and Setup

The primary control goal is to track the depth of cut to the specified surface profile. In circular cutting, this problem reduces to regulation since the desired shape is a constant radius. There are significant instrumentation difficulties in obtaining the cutting depth for output feedback. Tool position on the other hand is easy to measure using, for example, a linear digital encoder mounted to the linear motor. In the absence of lathe/workpiece structure flexibility, tool position is depth of cut. Even with such flexibility, tool position is still a close approximation of cutting depth since the lathe/workpiece typically has large static stiffness. Tool position will therefore be regulated instead of cutting depth. Because proportional-integral-derivative (PID) control has an obvious analogy to the passive system, it has been considered here for regulation as a first approach to active control.

The linear motor assembly is comprised of dual permanent magnet brushed motors with a combined output of 535 N rms continuous force, and 1605 N peak force. Digital implementation of the continuous PID control law was achieved using a first order forward difference for the derivative term, where h denotes the sampling period:

$$u(k) = K_p e(k) + K_d \frac{e(k) - e(k-1)}{k} + K_i \sum_{i=1}^{k} e(i)h \qquad (5.1)$$

The experimental cutting setup is depicted in Fig. 5.1, and a photograph of the actual system shown in Fig. 5.2. Tool position was measured with an optical encoder of 2 μm resolution mounted to the linear motor slide. The active control was implemented digitally by floating point arithmetic using a digital signal processor (TMS320C30).

For system identification purposes under noncutting conditions, an external disturbance d_t representing the cutting force was introduced as a voltage input to the power amplifier. Figure 5.3 shows the experimental servo loop frequency response y_t/d_t for a particular PD control law. It is observed that the stiffness (i.e., inverse of frequency response magnitude) increases as frequency increases and a ditch of stiffness at the resonant frequency does not exist because of the imposed large active damping. The experimental data fit well to a 2nd order transfer function:

$$\frac{y_t}{d_t} = 0.04095 \frac{1 - \frac{s}{1101.9}}{s^2 + 503.8\ s + 52171.9}\ \text{(m/N)} \qquad (5.2)$$

Note that the zero may be reasonably neglected. Equating the characteristic equations of (3.16) and (5.2) (i.e., under noncutting conditions, $K_c = K_{cd} = 0$), the following effective system parameters have been determined:

$$m_t = 19.5\ \text{kg} \qquad B_t = 2007\ \text{N·s/m}$$

Figure 5.4 shows the experimentally obtained achievable static stiffness data as a function of the digital control sample rate. For a given damping ratio, peak stiffness occurs in the range of 1500 to 2000 Hz. A sample rate of 1800 Hz has therefore been chosen for all control implementation. Some perspective may now be made on the utility of the motor as a

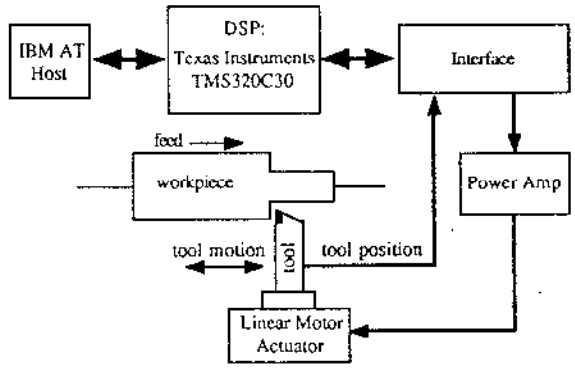

Fig. 5.1 Linear motor actuated cutting setup (depicting axial configuration)

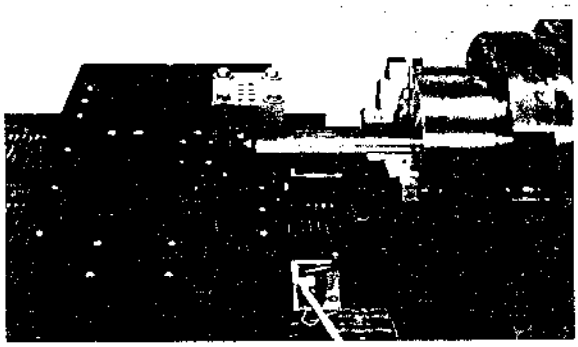

Fig. 5.2 Experimental setup in laboratory

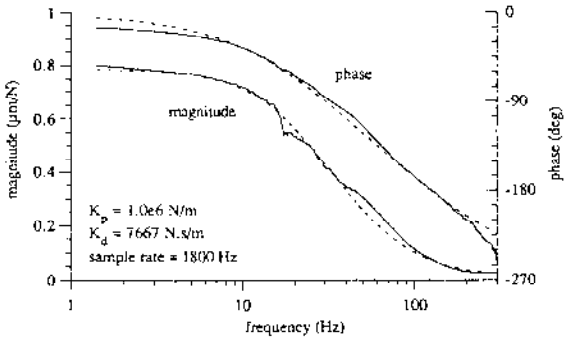

Fig. 5.3 PD controlled linear motor frequency response plots of y_t/d_t (solid = experimental, dashed = 2nd order fit)

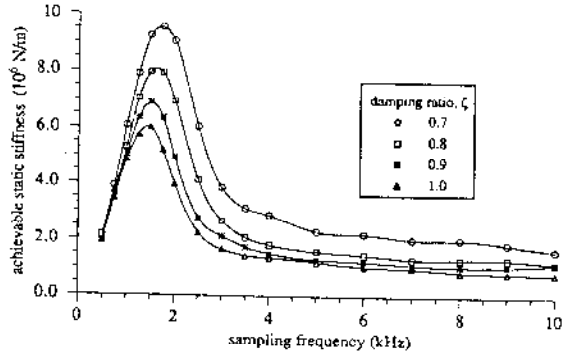

Fig. 5.4 Achievable closed loop static stiffness, PD control

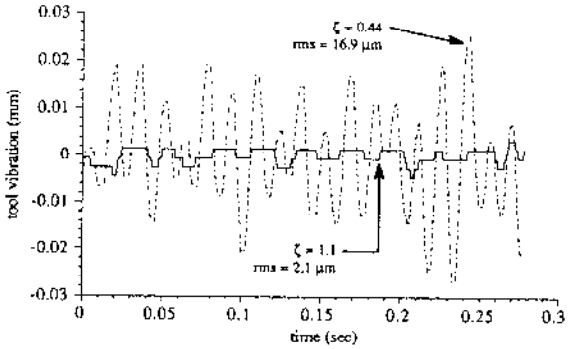

Fig. 5.6 Stable cutting tool response for two damping ratios, PD control, feedrate = 0.091 mm/rev, spindle speed = 1100 rpm, d_{cut} = 2.03 mm

Table 5.5 Minimum required static stiffness for PD-control cutting stability of different materials

Material	Specific energy * u_0 (approximate) (N/m^2)	$K_{c,axial}$ ** d_{cut} = 2 mm (N/m)	min. required static stiffness: eqn. (3.10) (N/m)	eqn. (3.18) μ=1, ζ=1 (N/m)
aluminum alloy	0.70 x 10^9	0.70 x 10^6	1.40 x 10^6	0.18 x 10^6
free-machining brass	1.06 x 10^9	1.06 x 10^6	2.12 x 10^6	0.27 x 10^6
mild steel (AISI 1018)	2.10 x 10^9	2.10 x 10^6	4.20 x 10^6	0.53 x 10^6
stainless steel (416F)	2.76 x 10^9	2.76 x 10^6	5.52 x 10^6	0.69 x 10^6
high-temp. alloys (Ni or Co based)	4.90 x 10^9	4.90 x 10^6	9.80 x 10^6	1.23 x 10^6

* Specific energy data taken from (Shaw, 1984), except 416F stainless steel, which was experimentally determined.
** $K_{c,axial} = (u_0 \times d_{cut})/2$

feed drive under PD control. Table 5.5 gives the minimum static stiffness requirements for stability with a particular set of cutting conditions, as independently determined by Eqs. (3.10) and (3.18). When interpreting the application of (3.10), static stiffness may be treated equivalent to dynamic stiffness if it is assumed that the servo loop has no resonant peaks in its frequency response. Comparison with Fig. 5.4 shows the minimum required stiffness values to fall below the maximum achievable stiffness of the hardware at hand ($\approx 6.0 \times 10^6$ N/m for $\zeta = 1.0$). It is interesting to note that under the specified conditions, sufficient only condition (3.10) computes a required stiffness value 8 times larger than that of necessary and sufficient condition (3.18).

Cutting tool regulation was alternately performed in both the axial and radial directions of motion, with the lathe drive used to feed the workpiece past the tool. In order to simplify analysis of the control system performance, it is desirable to minimize variation in the cutting process during experimental testing. The axial cutting configuration, while not actively effecting radial surface finish, exactly imposes $\mu = 1$ regardless of feedrate or cutting insert geometry. It thus offers analysis advantages over the radial configuration, for which μ is typically uncertain. Except where otherwise noted, all experimental cutting (axial and radial) was performed with the following common conditions:

material: 416F stainless steel, free machining
cutting velocity = 2 m/s
tool side rake = + 5 deg
workpiece chucked one end only
cutting insert: Carboloy TPG 322
motor static stiffness = $m_t \cdot \omega_n^2$ = 1e6 N/m
tool back rake = 0 deg
effective workpiece length = 88 mm

The static cutting stiffness was estimated as a function of cutting velocity by a series of dynamometer tests (not shown). For simplicity, the dynamic cutting stiffness, K_{cd}, was assumed to be zero. For a cutting velocity of 2 m/s, the following material cutting stiffness was calculated for the axial direction:

$$K_{c,axial} = \frac{\text{axial direction cutting force}}{\text{feed per revolution}} = 2.76\text{e}6 \text{ N/m}$$

PID control gains may now be chosen according to (3.19) to achieve desired closed loop properties. Spindle speed is set so that the cutting velocity (v) is at the specified value of 2 m/s at the radial center of the cut:

$$\text{spindle speed} = \frac{\text{cutting velocity}}{\text{workpiece radius}} = \frac{v}{\frac{d_w - d_{cut}}{2}} \cdot \frac{60}{2\pi} \text{ (rpm)} \quad (5.3)$$

For d_w relatively larger than d_{cut}, the effect of cutting velocity variation along the (radial axis) edge of the tool is negligible since the cutting velocity profile is essentially constant. However, as workpiece diameter is reduced, large variation exists in the velocity profile (e.g., for the worst case of $d_w = 2d_{cut}$, the velocity profile varies from $2v$ at the radially outermost point to zero at the innermost point!). Therefore, the above computed cutting stiffnesses lose accuracy. Although this inherent difficulty cannot easily be remedied, it should be remembered when interpreting experimental results.

5.1 PD and PID Control—Axial Configuration Regulation Results. Figure 5.6 shows tool vibration under stable cutting for two different tool damping ratios, in which the static tool displacement has been removed from the figure. The higher damped case has an rms vibration level 8 times less than that of the more lightly damped case. This is due to the fact that increasing the damping increases the minimum value of dynamic stiffness. The rms value has been calculated after removal of the signal DC component (as will be the case throughout the remainder of this paper). Note that the squared shape of the $\zeta = 1.1$ response is caused by the finite resolution of the position encoder.

The following control cases will now be investigated:

Case A: PD control, feedrate = 0.1 mm/rev, $\zeta = 1.1$
Case B: PD control, feedrate = 0.2 mm/rev, $\zeta = 1.1$
Case C: PD control, feedrate = 0.1 mm/rev, $\zeta = 0.28$
Case D: PID control, feedrate = 0.1 mm/rev, $\zeta = 1.1$, a is detailed in results

Figure 5.7 illustrates the chatter control capabilities of active damping. While Case A shows stable cutting, the lighter damped Case C displays chatter. Figure 5.8 shows Case C over a longer time window. The modulated growth of cutting chatter is here more readily visible. Case B demonstrates the effect of doubling the feedrate over that of Case A, generating a three fold increase in tool rms vibration. Power spectral densities are shown in Fig. 5.9. The strong power components at the spindle frequency and twice this frequency suggests the presence of spindle runout or workpiece out-of-roundness. In addition, the unstable Case C displays a highly dominating power

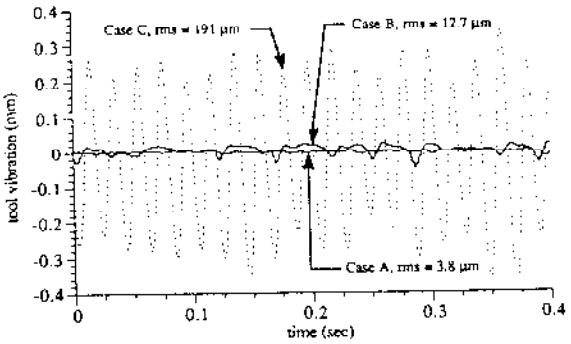

Fig. 5.7 Stable and unstable cutting time responses spindle speed = 1072 rpm, $d_{cut} = 2.03$ mm

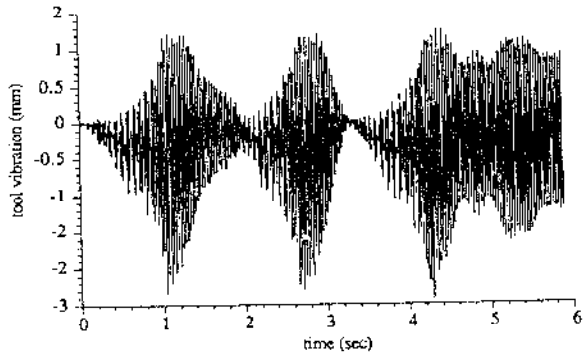

Fig. 5.8 Unstable cutting showing chatter growth for Case C, spindle speed = 1072 rpm, d_{cut} = 2.03 mm

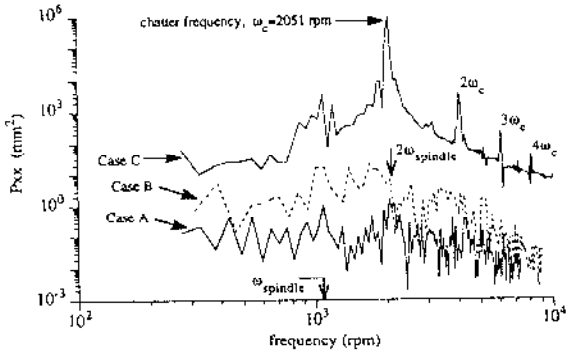

Fig. 5.9 Power spectral density, cutting cases A, B, and C. Spindle speed = 1072 rpm, d_{cut} = 1.78 mm

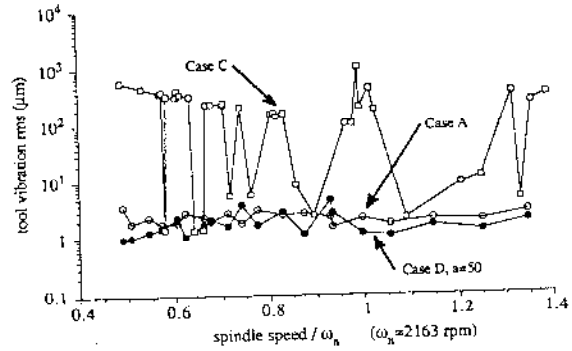

Fig. 5.10 Tool vibration rms vs spindle speed ratio, d_{cut} = 1.78 mm

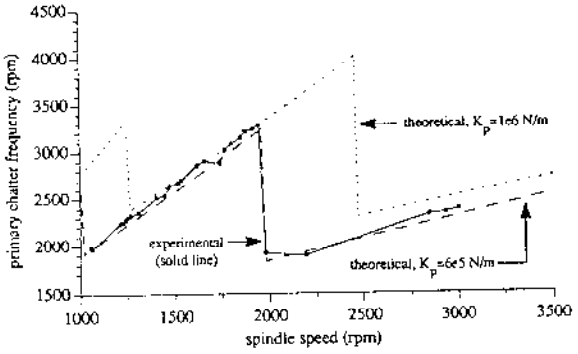

Fig. 5.11 Primary chatter frequency vs. spindle speed for Case C, d_{cut} = 1.78 mm

component at the chatter frequency, and lesser peaks at integer multiples of this frequency.

Figure 5.10 shows rms tool vibration as a function of spindle speed for Cases A, C, and D. This graph is qualitatively related to the stability chart of Fig. 3.3 in that tool vibration is sensitive to spindle speed, and more so for the lower damping ratio Case C. Equation (3.18) predicts the following asymptotic limits on K_c for stable (PD) cutting with $m_t \cdot \omega_n^2 = 1e6$ N/m:

$$\zeta \simeq 1.1 \Rightarrow K_c < 4.62e6 \text{ N/m} \quad \zeta = 0.28 \Rightarrow K_c < 0.72e6 \text{ N/m}$$

Since $K_{c,axial}$ was estimated at 2.76e6 N/m, it is to be expected that the lower damping Case C chatters at certain spindle speeds, while the more highly damped Case A (and D) does not. Additionally, it is seen that at most spindle speeds, the PID Case D has less vibration than the related PD Case A.

If one follows the heuristic argument that operating with a larger stability margin leads to less tool vibration, one would expect the vibration sensitivity to spindle speed for Case C to be reduced for speed ratios greater than about 1.1 (see Fig. 3.3). However, Case C displays continued vibration variation in the speed range of 1.2 to 1.4. This may be attributed to lathe/workpiece dynamics, as suggested by Fig. 4.1, and also due to the fact that relatively small workpiece diameters are necessary to achieve this speed ratio, and thus cutting velocity is no longer constant across the tool face (as discussed in Section 5).

Finally, as a means of model verification, the dominant chatter frequency of Case C for various spindle speeds is compared with the predicted theoretical values, shown in Fig. 5.11. Theoretical values were obtained as the phase-crossover frequency on the Nyquist chart of Eq. (3.17), and thus correspond to a system operating at the lobed stability limit. Even though the K_c value of the lobed limit will not generally equal the actual value of K_c, the limiting case provides a good estimate since chatter frequency is relatively insensitive to changes in K_c. The experimental data is best predicted by a theoretical model with stiffness value of 6e5 N/m, rather than with the actual servo stiffness of 1e6 N/m. One possible explanation for this lies in the lathe/workpiece flexibility previously neglected by (3.17), which will reduce the effective stiffness of the system.

5.2 PD and PID Control—Radial Configuration Regulation Results. As previously stated, the radial cutting configuration directly affects final surface finish, and is thus of primary interest for industrial applications. Figure 5.12 shows the cutting time response for three different integral mode values of "a". With $a = 0$ (i.e., PD control), the tool undergoes a steady-state static deflection equivalent to 4.7 percent of the nominal cutting depth. The other two cases, having the integral mode active, display zero steady-state deflection. As expected, the integral mode of control is desirable for precision machining. It is also seen that rms tool vibration is greatest for the $a = 0$ case, although a comparable vibration level exists for $a = 100$. In practice, the integral mode gain (i.e., "a") should not be made too large if robustness is to be maintained, and to avoid integral windup.

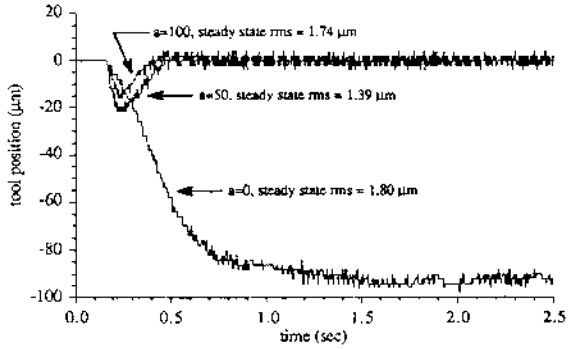

Fig. 5.12 Stable tool motion during radial configuration cutting, Case D, spindle speed = 1136 rpm, d_{cut} = 2.03 mm

6 Conclusion

The purpose of this paper was to investigate active control of direct drive linear motors for the turning process. The following conclusions can be drawn from this study: (*i*) A cutting system dynamic model, comprised of three feedback loops, has been developed for stability analysis purposes. (*ii*) The interaction of the cutting process with the tool servo loop has been shown to have significant instability consequences in systems with small drive gear reductions. (*iii*) Various necessary and sufficient conditions for stability have been derived and have been used to study the effect of damping and gear reduction in system stability. (*iv*) The stability advantage of the active linear motor cutting system stems from its ability to increase system damping while still maintaining sufficient static stiffness.

Experimental results have shown the promising potential of linear motors as feed drives in the turning process. The specific linear motor direct-drive used in this research is clearly able to maintain stability in the servo/cutting process loop, and it may be expected that such capabilities are reflective of this type of actuator in general. The present experimental choice for closed loop static stiffness of 1e6 N/m is rather conservative. Significant margin exists in the hardware to increase this stiffness value if cutting conditions so demand. In addition, more advanced servo controllers than the PID type may be able to achieve even higher stiffness capabilities.

Stability is thus not a problematic issue in using linear motor drives for turning, and attention may now be turned to the important performance issues of disturbance rejection and trajectory tracking. Such issues are of industrial significance in the production of precision machined parts, and it is in these areas that direct drives will really be able to exhibit their advantages and worth.

Acknowledgment

This research was supported in part by National Science Foundation under Grant No. DDM90-09830.

References

Barkman, W. E., 1980, "Drive Controls," *Technology of Machine Tools, Volume 4: Machine Tool Controls*, Lawrence Livermore Research Lab, University of California.

Comstock, T. R., Tse, F. S., and Lemon, J. R., 1969, "Application of Controlled Mechanical Impedance for Reducing Machine Tool Vibrations," ASME JOURNAL OF ENGINEERING FOR INDUSTRY, Vol. 91, pp. 1057–1062.

Desoer, C. A., and Vidyasagar, M., 1975, *Feedback Systems: Input-Output Properties*, Academic Press, New York, pp. 40–45.

Gurney, J. P., and Tobias, S. A., 1961, "A Graphical Method for the Determination of the Dynamic Stability of Machine Tools," *Int. J. of Machine Tool Design & Research*, Vol. 1, pp. 148–156.

Matsubara, T., Yamamoto, H., and Mizumoto, H., 1985, "Study on Regenerative Chatter Vibration with Dynamic Cutting Force," *J. of Japan Society of Precision Engineering*, Vol. 19, No. 4, pp. 260–265.

Merritt, H. E., 1965, "Theory of Self-Excited Machine Tool Chatter," ASME JOURNAL OF ENGINEERING FOR INDUSTRY, Vol. 87, No. 4, pp. 447–454.

Mitchell, E. E., and Harrison, E., 1977, "Design of a Hardware Observer for Active Machine Tool Control," ASME *Journal of Dynamic Systems, Measurement, and Control*, Vol. 99, pp. 227–232.

Mitchell, E. E., and Harrison, E., 1974, "Active Machine Tool Controller Requirements for Noise Attenuation," ASME JOURNAL OF ENGINEERING FOR INDUSTRY, Vol. 96, pp. 261–267.

Nachtigal, C. L., and Cook, N. H., 1970, "Active Control of Machine Tool Chatter," *J. of Basic Engineering*, Vol. 92, pp. 238–244.

Nachtigal, C. L., 1972, "Design of a Force Feedback Chatter Control System," ASME *Journal of Dynamic Systems, Measurement, and Control*, Vol. 94, pp. 5–10.

Shaw, M. C., 1984, *Metal Cutting Principles*, Oxford University Press, New York, p. 43.

Smith, S., and Tlusty, J., 1990, "Update on High-Speed Milling Dynamics," ASME JOURNAL OF ENGINEERING FOR INDUSTRY, Vol. 112, No. 2, pp. 142–149.

Srinivasan, K., 1982, "Application of the Regeneration Spectrum Method to Wheel Regenerative Chatter in Grinding," ASME JOURNAL OF ENGINEERING FOR INDUSTRY, Vol. 104, pp. 46–54.

Srinivasan, K., and Nachtigal, C. L., 1978, "Analysis and Design of Machine Tool Chatter Control Systems Using the Regenerative Spectrum," ASME *Journal of Dynamic Systems, Measurement, and Control*, Vol. 100, pp. 191–200.

Thompson, R., 1986, "Chatter Growth—Tests to Evaluate Theory," *Symposium on Modeling, Sensing, and Control of Manufacturing Processes*, ASME DSC-Vol. 4, pp. 205–219.

APPENDIX A

Derivation of Eq. (3.14)

Let the complex number $K_c T(j\omega) := a + jb$. Then (3.13) yields the condition

$$(\alpha^2+\beta^2)^{1/2} < \frac{1}{\mu}\left[(1+\alpha)^2+\beta^2\right]^{1/2}, \quad 0 \le \mu \le 1 \tag{A.1}$$

$$\Rightarrow \quad \mu^2[\alpha^2+\beta^2] < 1+2\alpha+\alpha^2+\beta^2 \tag{A.2}$$

$$\Rightarrow \quad \alpha^2+\beta^2+\frac{2\alpha+1}{1-\mu^2} > 0$$

$$\Rightarrow \quad \left[\alpha^2+\frac{1}{1-\mu^2}\right]^2+\beta^2+\frac{1}{1-\mu^2}-\left[\frac{1}{1-\mu^2}\right]^2 > 0$$

$$\Rightarrow \quad \left[\alpha^2+\frac{1}{1-\mu^2}\right]^2+\beta^2 > \left[\frac{\mu}{1-\mu^2}\right]^2 \tag{A.3}$$

from which (3.14) immediately follows.

APPENDIX B

Derivation of Eq. (3.18)

Arrange the characteristic equation of (3.17) into the form

$$1+\frac{-\dfrac{\mu K_c}{m_t}e^{-\tau s}}{s^2+2\zeta\omega_n s+\left(\omega_n^2+\dfrac{K_c}{m_t}\right)} = 1+G(s)e^{-\tau s} = 0 \tag{B.1}$$

Since both $G(s)$ and $e^{-\tau s}$ and $e^{-\tau s}$ are stable transfer functions, the small gain theorem gives the necessary and sufficient stability condition that the loop gain be less than 1. If this condition is not met, then there exists some τ (i.e., spindle speed) which makes the system unstable. Since the delay term always has magnitude 1, the condition reduces to $|G(j\omega)| < 1$. The second order system $G(s)$ has maximum magnitude

$$\frac{\mu K_c}{m_t}\frac{1}{2\bar{\omega}_n^2\,\bar{\zeta}\sqrt{1-\bar{\zeta}^2}} \quad \text{if } \bar{\zeta} \le \frac{1}{\sqrt{2}}, \quad \bar{\omega}_n^2 := \omega_n^2+\frac{K_c}{m_t}, \quad \bar{\zeta} := \zeta\frac{\omega_n}{\bar{\omega}_n}$$

If $\bar{\zeta} > 1/\sqrt{2}$, the maximum magnitude is $\mu K_c/m_t\bar{\omega}_n^2$, which may be shown less than the lower damped case. Assume that the critical K_c value gives the lower damping ratio case, and equate the transfer function maximum magnitude to unity:

$$\mu K_c < 2m_t\bar{\omega}_n^2\,\bar{\zeta}\sqrt{1-\bar{\zeta}^2}$$

After substantial manipulation, one obtains the following:

$$\mu^2 K_c^2 - 4m_t\omega_n^2\zeta^2 K_c + 4m_t^2\omega_n^4\zeta^2(\zeta^2-1) = 0 \qquad \text{(B.2)}$$

The quadratic formula shows that (B.2) always has real roots in the μ range of interest ($0 \le \mu \le 1$). Manipulation of the larger of the two roots yields Eq. (3.18). It remains to show valid at the critical K_c value the assumption

$$\bar{\zeta} \le \frac{1}{\sqrt{2}} \iff \zeta\sqrt{\frac{\omega_n^2}{\omega_n^2 + K_c/m_t}} \le \frac{1}{\sqrt{2}}$$

Substituting (3.18) into the above yields the condition

$$(2\zeta^2-1)\mu^2 \le 2\zeta^2 + 2\zeta[\mu^2 + \zeta^2(1-\mu^2)]^{1/2} \qquad \text{(B.3)}$$

For $0 \le \mu \le 1$, the left-hand side of (B.3) is always $\le 2\zeta^2$, which in turn is always less than or equal to the right-hand side. Thus, the inequality holds, and the assumption is valid.